JOURNAL OF COMPUTATIONAL PHYSICS 9, 167–193 (1972)

Numerical Solutions of Reactive Fluid Flows During Postignition Transients in Hybrid Rocket Systems

W. S. Y. HUNG,* C. S. CHEN,† AND J. K. HAVILAND‡

School of Engineering and Applied Science,
University of Virginia, Charlottesville, Virginia, 22901

Received May 25, 1971

A computational method has been developed for the study of the postignition transients in hybrid rocket systems. The particular system chosen consisted of a gaseous oxidizer flowing within a tube of solid fuel, resulting in heterogeneous combustion. With the appropriate assumptions, two-dimensional, time-dependent conservation equations were derived for the reacting gas phase, and for the solid phase, in a cylindrical coordinate system. These were then programmed for numerical computation, using two implicit finite-difference schemes, the Lax–Wendroff scheme for the gas phase, and the Crank–Nicolson scheme for the solid phase. Appropriate initial and boundary conditions were represented, including heat and mass conservation at the interface between gas and solid. Initially, no attempt was made to relate the recession rate at the surface to the surface temperature, or to include heat transfer by radiation. A simple case was selected for preliminary calculations, with aluminum and oxygen as fuel and oxidizer, and aluminum oxide as the product. Although no transient experimental data was available for comparison, good qualitative agreement with available steady-state data was noted.

INTRODUCTION

This paper covers the development and preliminary applications of a computer solution for the initial combustion transient in a hybrid rocket system consisting of a solid fuel and a liquid oxidizer. One of the major advantages of the hybrid rocket systems over the conventional solid or liquid rocket systems is their relative safety from accidental ignition. Although several previous studies [1–9] have been made of regression rates during steady combustion, almost no efforts have been

* Senior Scientist, Research Laboratories for the Engineering Sciences, University of Virginia, Charlottesville, Virginia.

† Assistant Professor, Department of Mechanical Engineering, University of Virginia, Charlottesville, Virginia.

‡ Professor, Department of Aerospace Engineering, University of Virginia, Charlottesville, Virginia.

581/9/2-1

made previously to gain a fundamental understanding of the nonsteady problems involved, of which the initial combustion transient during the postignition period is a prime example.

The current analysis adopts an overall approach with a view to gaining a basic understanding of the combustion processes involved in the hybrid rocket systems. The governing equations describing the physical system have been formulated in the most general way possible because a numerical solution of these equations is sought. Mathematical modeling of the physical mechanisms was performed for a simple case, with provisions for the incorporation of more sophisticated mathematical models in the future. This approach should eventually lead to a computational method capable of simulating more realistic hybrid combustion phenomena.

From published experimental work, it had been established that turbulent flows are characteristic of hybrid rocket systems. It was intended, therefore, to limit the analysis to turbulent flows. In order that the derived governing equations can be adopted for turbulent flows, the use of a phenomenological theory is implied. The transport properties are then strongly position dependent. In the process of development, however, certain simplifying assumptions have to be made to allow the handling of the numerical computational problems involved. To retain the coupling nature of the governing equations, no assumptions have been made on the state variables, such as temperature, density of the gas mixture, etc. Instead, properties that appear as coefficients in the various terms in the governing equations, such as viscosity, specific heat, etc., have been assumed constant to cut down the amount of computational time used while demonstrating the feasibility of the computational method.

This paper describes the mathematical formulation of the problem, outlines the numerical techniques used, defines a simple problem involving oxygen flowing through a tubular fuel block of aluminum, and presents the results from two early sets of calculations, one in which ignition subsided, and the other in which a steady-state combustion sustained itself. It concludes with a summary of plans for future development of this computational technique.

Initial computer calculations were performed on the Burroughs 5500 computer at the University of Virginia's Computer Science Center. The results reported in this paper were obtained on the CDC6400-6600 computers of the NASA Langley Research Center's Analysis and Computation Division.

Model for the Physical System

The following assumptions are made for the physical system: (a) All dependent variables are symmetric with respect to the θ direction in cylindrical coordinates:

(b) The effects of a physically receding fuel surface are neglected. A sketch of the physical system used is shown in Fig. 1.

The reason for assumption (a) was that although the advance of computer technology has made available computers with high speed and greater storage capacity, it is still not practical to attempt numerical solution of a three-dimensional transient problem. Therefore, a two-dimensional coordinate system was adopted for the present study.

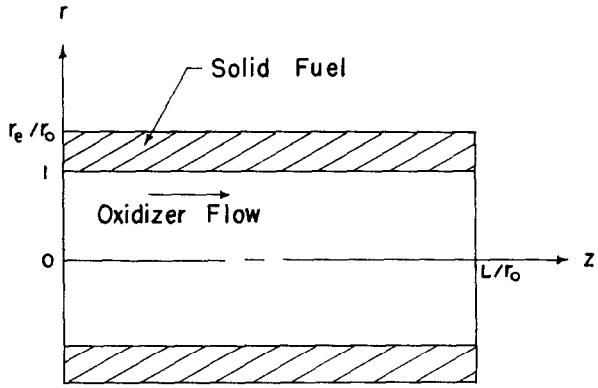

FIG. 1. The physical system.

MATHEMATICAL FORMULATION

A. *Model for the Gas Phase*

The gas phase in hybrid rocket systems generally consists of a nonisothermal multicomponent fluid of N chemical species. The general conservation equations for a multicomponent reacting gas mixture have been derived by Hirschfelder, Curtis, and Bird [10]. Following the approaches by Lees [11] and Chung [12] in formulating the equations for the mass, momentum, and energy fluxes, a set of governing equations for the gas phase in dimensionless form is derived as follows:

Continuity Equation

$$D\rho/Dt + \rho[(\partial v_r/\partial r) + (v_r/r) + (\partial v_z/\partial z)] = 0. \tag{1}$$

A complete list of symbols used in this section has been included at the end of this paper for cross reference.

Species Continuity Equations

$$\rho \frac{Dy_i}{Dt} = \frac{1}{ReSc}\left[\frac{\partial}{\partial r}\left(\rho D_i \frac{\partial y_i}{\partial r}\right) + \left(\frac{\rho D_i}{r}\right)\left(\frac{\partial y_i}{\partial r}\right) + \frac{\partial}{\partial z}\left(\rho D_i \frac{\partial y_i}{\partial z}\right)\right] + DaW_i, \quad i = 1, 2, \ldots, N. \tag{2}$$

Momentum Equations

$$\rho \frac{Dv_r}{Dt} = -\frac{\partial P}{\partial r} + \frac{1}{Re}\left\{\frac{2}{3}\frac{\partial}{\partial r}\left[\mu\left(2\frac{\partial v_r}{\partial r} - \frac{v_r}{r} - \frac{\partial v_z}{\partial z}\right)\right] + \frac{2}{3}\left(\frac{\mu}{r}\right)\left(2\frac{\partial v_r}{\partial r} - \frac{v_r}{r} - \frac{\partial v_z}{\partial z}\right) + \frac{\partial}{\partial z}\left[\mu\left(\frac{\partial v_z}{\partial r} + \frac{\partial v_r}{\partial z}\right)\right]\right\}, \tag{3}$$

$$\rho \frac{Dv_z}{Dt} = -\frac{\partial P}{\partial z} + \frac{1}{Re}\left\{\frac{\partial}{\partial r}\left[\mu\left(\frac{\partial v_z}{\partial r} + \frac{\partial v_r}{\partial z}\right)\right] + \frac{\mu}{r}\left(\frac{\partial v_z}{\partial r} + \frac{\partial v_r}{\partial z}\right) + \frac{2}{3}\frac{\partial}{\partial z}\left[\mu\left(2\frac{\partial v_z}{\partial z} - \frac{\partial v_r}{\partial r} - \frac{v_r}{r}\right)\right]\right\}. \tag{4}$$

Energy Equation

$$\rho C_p \frac{DT}{Dt} = Ec\frac{DP}{Dt} + \frac{1}{PrRe}\left[\frac{\partial}{\partial r}\left(\lambda\frac{\partial T}{\partial r}\right) + \frac{\lambda}{r}\frac{\partial T}{\partial r} + \frac{\partial}{\partial z}\left(\lambda\frac{\partial T}{\partial z}\right)\right] + \frac{1}{ReSc}\left[\rho\frac{\partial T}{\partial r}\left(\sum_i D_i C_{pi}\frac{\partial y_i}{\partial r}\right) + \rho\frac{\partial T}{\partial z}\left(\sum_i D_i C_{pi}\frac{\partial y_i}{\partial z}\right)\right] - Da\left(\sum_i h_i w_i\right). \tag{5}$$

Equation of State

$$P = \frac{1}{Ec}\sum_{i=1}^{N}(y_i R_i)\rho T. \tag{6}$$

The underlying assumptions in deriving this set of governing equations are as follows:

(a) Flow of N-component gas mixture with chemical reaction,
(b) Isotropic, heterogeneous media,
(c) Gravity and external forces negligible,
(d) Newtonian fluid with negligible bulk viscosity, i.e., $\mu_B \ll \mu$,
(e) Fourier's law for heat conduction,

(f) System is a binary mixture so far as diffusion is concerned such that Fick's law for diffusion is applicable,

(g) Negligible viscous dissipation, radiative and Dufour effects,

(h) Ideal gas mixture such that the enthalpy of the gas mixture h can be defined as follows:

$$h \equiv \sum_i (y_i h_i), \tag{7}$$

$$h_i \equiv \int_1^T C_{pi}\, dT + h_i^0 + h_{Li}\,. \tag{8}$$

It was pointed out by Bird, Steward, and Lightfoot [13] that Eqs. (1) and (2) constitute only N independent equations. For the numerical solution of this set of equations, it appears to be more convenient to eliminate Eq. (1). Hence, Eqs. (2)–(6) constitute the $(N + 4)$ independent equations in the gas phase to be solved.

B. *Model for the Solid Phase*

The main concern in the solid phase is its temperature distribution. Hence, the governing equation in the solid phase is the transient heat conduction equation

$$\rho_s C_s \frac{\partial T_s}{\partial t} = \frac{\alpha_{s0}}{r_0 v_0}\left[\frac{\partial}{\partial r}\left(\lambda_s \frac{\partial T_s}{\partial r}\right) + \frac{\lambda_s}{r}\left(\frac{\partial T_s}{\partial r}\right) + \frac{\partial}{\partial z}\left(\lambda_s \frac{\partial T_s}{\partial z}\right)\right]. \tag{9}$$

The restrictions imposed on this equation are as follows:

(a) Isotropic, heterogeneous media,

(b) Fourier's law for heat conduction,

(c) No heat source or sink.

C. *Model at the Gas-Solid Interface*

A balance of mass and energy is assumed at the gas-solid interface at any instant of time based on the general conservation principle

$$\begin{aligned}&[\text{Rate of Mass or Energy out}] - [\text{Rate of Mass or Energy in}]\\ &\quad = [\text{Rate of Mass or Energy Production}]\end{aligned} \tag{10}$$

The governing equations derived for the interface are as follows:

Mass Balance

$$\frac{D_0}{r_0 v_0}\left(\frac{\partial y_i}{\partial r}\right)_w \rho_w D_{iw} - \rho_w v_w y_{iw} = \left(\frac{\rho_{s0}}{\rho_0}\right)\left(\frac{\dot{r}_0}{v_0}\right)\rho_s \dot{r} y_{isw}, \qquad i = 1, 2, \ldots, N \tag{11}$$

Energy Balance

$$-\left(\frac{T_{s0}}{T_0}\right)\left(\frac{\lambda_{s0}}{\lambda_0}\right)\left(\lambda_s \frac{\partial T_s}{\partial r}\right)_w = \rho_w v_w \left(\frac{r_0 v_0}{\alpha_0}\right)\left(\sum_i (h_i y_i)_w\right) - \left(\lambda \frac{\partial T}{\partial r}\right)_w + \rho_{sw}\dot{r}\left(\frac{T_{s0}}{T_0}\right)\left(\frac{\lambda_{s0}}{\lambda_0}\right)\left(\frac{r_0 \dot{r}_0}{\alpha_{s0}}\right)\left[\sum_i (h_{sgi} y_{isw})\right] - \rho_w \left(\frac{D_0}{\alpha_0}\right)\left[\sum_i \left(h_i D_i \frac{\partial y_i}{\partial r}\right)_w\right]. \tag{12}$$

Numerical Methods Used

The governing equations in the gas phase may behave either as hyperbolic, or parabolic partial differential equations depending on whether the first-order spatial derivatives or the second-order spatial derivatives are the dominating terms, respectively. For turbulent flow ($Re > 2100$) the terms containing the second-order

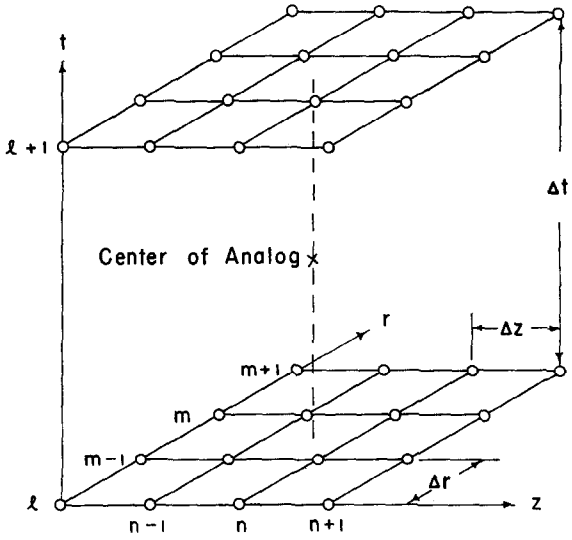

Fig. 2. Lax–Wendroff scheme.

spatial derivatives are small compared with those of the first-order spatial derivatives. Therefore, it was predicted that Eqs. (2)–(5) were most likely to behave as first-order hyperbolic partial differential equations, so that the Lax–Wendroff finite difference scheme [14] of the second-order accuracy was used for the numerical solution. The nomenclature used, and the center about which this numerical analog is based, are presented schematically in Fig. 2. The difference analogs for this scheme are derived as follows:

$$r(l+1/2, m-1/2, n-1/2) \simeq (m-3/2)(\Delta r), \tag{13}$$

$$\begin{aligned} u(l+1/2, m-1/2, n-1/2) \simeq [&u(l+1, m, n) + u(l+1, m, n-1) \\ &+ u(l+1, m-1, n) + u(l+1, m-1, n-1) \\ &+ u(l, m, n) + u(l, m, n-1) + u(l, m-1, n) \\ &+ u(l, m-1, n-1)]/8. \end{aligned} \tag{14}$$

$$\begin{aligned} \frac{\partial u}{\partial t}(l+1/2, m-1/2, n-1/2) \simeq [&u(l+1, m, n) + u(l+1, m, n-1) \\ &+ u(l+1, m-1, n) + u(l+1, m-1, n-1) \\ &- u(l, m, n) - u(l, m, n-1) - u(l, m-1, n) \\ &- u(l, m-1, n-1)]/4\Delta t, \end{aligned} \tag{15}$$

$$\begin{aligned} \frac{\partial u}{\partial r}(l+1/2, m-1/2, n-1/2) \simeq [&u(l+1, m, n) + u(l+1, m, n-1) \\ &- u(l+1, m-1, n) - u(l+1, m-1, n-1) \\ &+ u(l, m, n) + u(l, m, n-1) - u(l, m-1, n) \\ &- u(l, m-1, n-1)]/4/\Delta r, \end{aligned} \tag{16}$$

$$\begin{aligned} \frac{\partial u}{\partial z}(l+1/2, m-1/2, n-1/2) \simeq [&u(l+1, m, n) - u(l+1, m, n-1) \\ &+ u(l+1, m-1, n) - u(l+1, m-1, n-1) \\ &+ u(l, m, n) + u(l, m, n-1) + u(l, m-1, n) \\ &- u(l, m-1, n-1)]/4/\Delta z, \end{aligned} \tag{17}$$

$$\begin{aligned} \frac{\partial^2 u}{\partial r^2}(l+1/2, m-1/2, n-1/2) \simeq [&u(l+1, m+1, n) + u(l+1, m+1, n-1) \\ &- u(l+1, m, n) - u(l+1, m, n-1) \\ &- u(l+1, m-1, n) - u(l+1, m-1, n-1) \\ &+ u(l+1, m-2, n) + u(l+1, m-2, n-1) \\ &+ u(l, m+1, n) + u(l, m+1, n-1) \\ &- u(l, m, n) - u(l, m-1, n) - u(l, m-1, n) \\ &- u(l, m-1, n-1) + u(l, m-2, n) \\ &+ u(l, m-2, n-1)]/8/\Delta r/\Delta r, \end{aligned} \tag{18}$$

$$\frac{\partial^2 u}{\partial z^2}(l+1/2, m-1/2, n-1/2) \simeq [u(l+1, m, n+1) - u(l+1, m, n) - u(l+1, m, n-1) + u(l+1, m, n-2) + u(l+1, m-1, n+1) - u(l+1, m-1, n) - u(l+1, m-1, n-1) + u(l+1, m-1, n-2) + u(l, m, n+1) - u(l, m, n) - u(l, m, n-1) + u(l, m, n-2) + u(l, m-1, n+1) - u(l, m-1, n) - u(l, m-1, n-1) + u(l, m-1, n-2)]/8/\Delta z/\Delta z. \tag{19}$$

These difference analogs were used to derive the difference forms for Eqs. (2)–(5).

Since Eq. (9) is a parabolic partial differential equation, the Crank–Nicolson finite difference scheme [14] was selected in deriving its difference form. Figure 3 shows the center about which this numerical analog is based. The difference analogs for the Crank–Nicolson scheme are as follows:

$$r(l+1/2, m, n) \simeq m(\Delta r), \tag{20}$$

$$u(l+1/2, m, n) \simeq [u(l+1, m, n) + u(l, m, n)]/2, \tag{21}$$

$$\frac{\partial u}{\partial t}(l+1/2, m, n) \simeq [u(l+1, m, n) - u(l, m, n)]/\Delta t, \tag{22}$$

$$\frac{\partial u}{\partial r}(l+1/2, m, n) \simeq [u(l+1, m+1, n) + u(l, m+1, n) - u(l+1, m-1, n) - u(l, m-1, n)]/4/\Delta r, \tag{23}$$

$$\frac{\partial u}{\partial z}(l+1/2, m, n) \simeq [u(l+1, m, n+1) + u(l, m, n+1) - u(l+1, m, n-1) - u(l, m, n-1)]/4/\Delta z, \tag{24}$$

$$\frac{\partial^2 u}{\partial r^2}(l+1/2, m, n) \simeq [u(l+1, m+1, n) + u(l, m-1, n) - 2u(l+1, m, n) - 2u(l, m, n) + u(l+1, m-1, n) + u(l, m-1, n)]/2/\Delta r/\Delta r, \tag{25}$$

$$\frac{\partial^2 u}{\partial z^2}(l+1/2, m, n) \simeq [u(l+1, m, n+1) + u(l, m, n+1) - 2u(l+1, m, n) - 2u(l, m, n) + u(l+1, m, n-1) + u(l, m, n-1)]/2/\Delta z/\Delta z. \tag{26}$$

Since Eqs. (11) and (12) do not have time derivative terms, these equations need

only to be satisfied at any instant of time. Thus, the difference forms of these equations are derived by using a time-independent finite difference scheme:

$$\frac{\partial u}{\partial r}(l, 1/2, n) = [u(l, 1, n) - u(l, 0, n)]/\Delta r \tag{27}$$

All difference equations were programmed in the Fortran IV language and run on a CDC 6600 computer. Since the numerical schemes employed are implicit, an iterative procedure had to be used. Because these coupled equations are slow in convergence it was necessary to employ a relaxation procedure, and to use

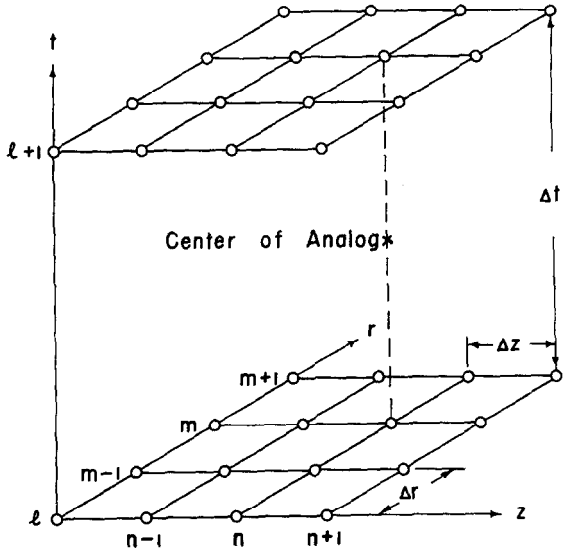

FIG. 3. Crank–Nicolson scheme.

Aitken's δ^2 method [15] as an accelerating convergence procedure, during the iterations at each time level, to speed up the calculations. The convergence criteria used, and the critical time increment, were determined by a trial process.

SOLUTION FOR A SIMPLE CASE

In order to gain insight into the numerical and the computational problems involved, it was decided to solve a simple case with the number of chemical species present in the gas phase kept to a minimum ($N = 3$). Because aluminum is considered as one of the potential chemical propellants, it was selected as the fuel,

and oxygen as the oxidizer, resulting in the production of aluminum oxide. The following describes the mathematical models, the initial, boundary and physical conditions, thermo-physical and transport properties, physical dimensions, and grid layout.

A. *Regression Rate of Fuel*

The regression rate of fuel has been the main concern in the previous analyses of hybrid rocket systems. In order to test out the numerical technique for the present study, it was felt that a simplified model for the regression rate of fuel should be adopted for the preliminary calculations. While the position of the fuel surface is assumed to be fixed, geometrically, constant mass addition of fuel from the fuel surface is assumed:

$$\dot{r} = \text{constant}. \tag{28}$$

Experimental data on the regression rates of various metalized hybrid fuel systems were reviewed [24, 25]. As a result the value of 0.0008 ft/sec was selected for the regression rate of fuel to be consistent with the nonreceding fuel surface model.

B. *Chemical Reaction Model*

(a) The gas-phase chemical reaction can be represented by a single overall irreversible chemical reaction such as fuel + oxidizer → product. According to Wilson [16], the gas-phase chemical reaction for the aluminum–oxygen system yields liquid aluminum oxide:

$$2\mathrm{Al} + (3/2)\mathrm{O}_2 \rightarrow \mathrm{Al}_2\mathrm{O}_3\,. \tag{29}$$

Since the current computational method cannot conveniently handle the problem of liquid droplet formation, this effect is assumed to be negligible.

(b) When the fuel-oxidizer ratio remains in the flammability limits, the rate of production of species for this overall reaction is calculated in the same manner as that for an elementary chemical reaction

$$W_i = \frac{M_i}{W_0}(\nu_i'' - \nu_i')\, k \prod_{j=1}^{N} \left(\frac{\rho y_i}{M_j}\right)^{\nu_j'}, \tag{30}$$

where ν_i' and ν_i'' are the stoichiometric coefficients for species i appearing as a reactant and as a product, respectively. The flammability limits for hydrocarbon fuels with air are in the range of 0.5 to 3.5, therefore, for lack of better data, these

values were used for the aluminum-oxygen system, expressed as the fuel-oxidizer ratio divided by that for a stoichiometric mixture.

(c) The rate constant k is estimated from the collision theory. For bimolecular reaction, the rate constant can be estimated as follows:

$$k = S\sigma_{12}^2[8\pi RT(M_1 + M_2)/M_1/M_2]^{1/2} \exp(E/RT), \tag{31}$$

where S is the steric factor, σ_{12} is the average diameter of colliding species and E is the activation energy.

From collision theory, the steric factor is the probability that a colliding pair will be oriented favorably for reaction. Hence, it should be a number equal to or less than unity. Since the value for the steric factor cannot be determined by empirical means through lack of experimental data on aluminum-oxygen gas-phase reaction, a value equal to unity has been chosen.

The average diameter of colliding species may be expressed as the sum of the effective radii of the colliding aluminum atom and oxygen molecule. The effective radius for aluminum is 1.43 Å [27] and the selected effective diameter of oxygen molecule is 3.43 Å [10].

From the collected data of activation energies for various complex gas-phase reactions [28], a value of 50 kcal/g-mole has been selected as the activation energy for the aluminum-oxygen gas-phase reaction.

C. *Initial and Boundary Conditions*

(a) The initial temperature profile corresponds to the conditions when ignition has just been completed;

(b) A fully developed flow of oxidizer reaches the inlet of the combustion chamber, such that the axial component of the velocity distribution at the inlet is based on the (1/7)-power law for turbulent flow, i.e.,

$$v_z = (1 - r)^{1/7}; \tag{32}$$

(c) The temperature at the exterior surface of the solid fuel is constant;

(d) The axial component of velocity is zero at the gas-solid interface and the radial component of velocity is zero at the center line.

D. *Pressure Gradient*

The static pressure over the entire flow field needs to be specified to correspond to a realistic physical situation. Numerical solution also requires specification of chamber pressure. Jones and Isaacson [17] have found experimentally that both

mass injection and combustion increase the axial pressure gradient. Therefore, the present study imposes a constant favorable downstream pressure gradient (0.164 psf/ft) similar to that used by Jones and Isaacson in their analysis.

E. *Thermo-physical and Transport Properties*

Properties were assumed to be independent of temperature and position, resulting in (a) constant transport properties by using equivalent turbulent values; (b) constant fluid properties; (c) constant properties for solid fuel. No emphasis was placed on the accuracy of the property values chosen; therefore the property values were estimated if they were not readily available.

The selected thermophysical properties for aluminum, oxygen, and aluminum oxide were obtained from previous experiments [18–22] and are summarized in Table I.

The eddy viscosity of a fully established turbulent flow through a pipe was measured experimentally by Rothfus, Archer, and Sikchi [23]. An average value for the eddy viscosity across a pipe was estimated to be approximately 20 times

TABLE I

Selected Thermophysical Properties for Aluminum, Oxygen, and Aluminum Oxide

		Al	O_2	Al_2O_3
Molecular wt. (lb_m/mole)		26.98 [18]	32.0 [18]	101.96 [18]
$\bar{C}_p$ (Btu/lb_m/°R)		0.26 [19]	0.295 [20]	0.27 [21]
$\bar{h}°$ (Btu/lb_m)		0	0	−7110.0 [22]
Boiling point (°R)		4932.3 [22]	162.34 [22]	6840.0 [22]
$\bar{h}_L$	$\bar{h}_{sl}$[a] (Btu/lb_m)	170.0 [22]	—	510.0 [22]
	$\bar{h}_{lg}$[a] (Btu/lb_m)	4710.0 [22]	—	2590.0 [22]
$\bar{\rho}_s$ (lb_m/ft^3)		168.5 [22]	—	—
$\bar{\lambda}_s$ (Btu/hr/ft/°R)		122.0 [22]	—	—
$\bar{C}_s$ (Btu/lb_m/°R)		0.221 [22]	—	—

[a] h_{sl} = heat of fusion; h_{lg} = heat of vaporization.

that due to molecular transport. Hence, a value equal to 0.0008 lb_m/sec/ft was selected for the viscosity of the gas mixture. The selected values for the binary diffusion coefficient and the thermal conductivity are 0.00592 ft^2/sec and 1.2 Btu/hr/ft/°R, respectively, such that Sc and Pr are approximately unity.

F. *Choice of Physical Dimensions*

The following restrictions were observed in selection of physical dimensions such as interior chamber radius r_0, exterior chamber radius r_e, chamber length L, chamber pressure P, and flow velocity v_0: (a) values chosen to be realistic, (b) the Mach number to be small, (c) the Reynolds number to correspond to turbulent flow. Physical dimensions finally selected were $r_0 = 0.25$ ft, $r_e = 0.2875$ ft, $L = 0.09$ ft, $P = 10$ atm and $v_0 = 20$ ft/sec.

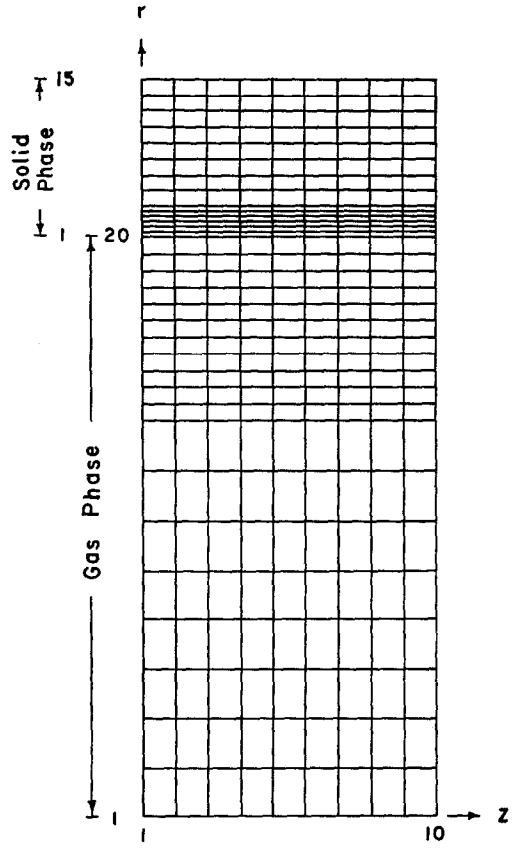

FIG. 4. Grid layout.

G. *Grid Layout*

The grid layout selected for these calculations is shown in Fig. 4. There were 10 equally spaced stations along the axis in the z direction. In the r direction, there were 20 stations in the gas phase and 15 stations in the solid phase. Finer grid size was employed near the gas–solid interface.

Results and Discussions

A. *Initial Profiles for Dependent Variables*

In assigning the initial values to the dependent variables, it was discovered that the energy balance at the interface was unreal. When an initial temperature profile in the solid phase was put in the transient temperature calculation, a relatively low temperature value at the interface was obtained due to high thermal conductivity of aluminum. This problem, presumably, could have been mitigated if an additional

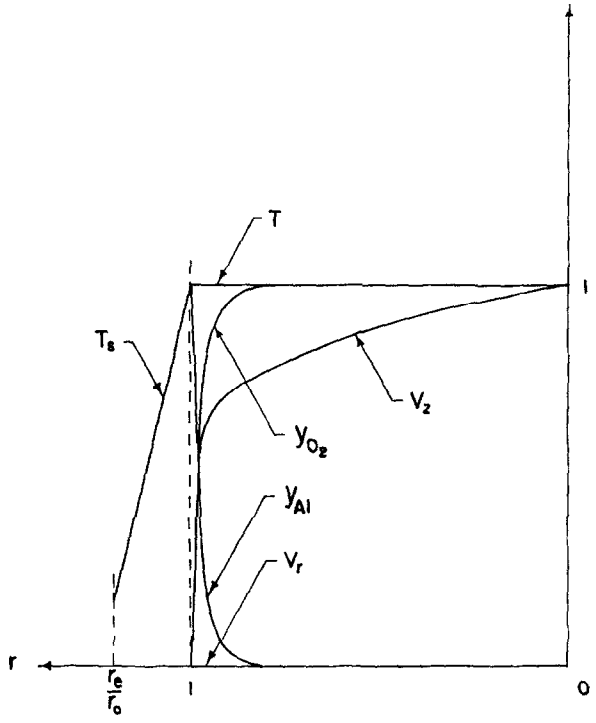

FIG. 5. Initial profiles at inlet, $z = 0$.

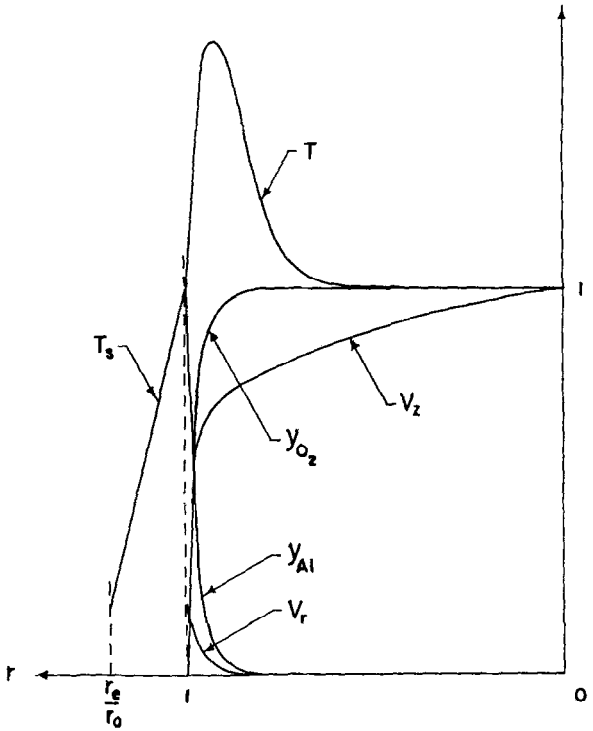

FIG. 6. Initial profiles at any axial position, $z > 0$.

energy production term due to radiative heat transfer were included in the energy equation. In the meantime, in order to maintain a realistic temperature value at the interface, the initial temperature profile in the solid phase was assumed to be that for the steady-state case at the start of the combustion process. Initial profiles of the dependent variables, v_r, v_z, T, T_s, y_{Al} and y_{O_2} at the inlet and at any other axial position are shown in Figs. 5 and 6, respectively.

B. *First Set of Calculations—Flame Subsided*

Using the convergence criteria, the critical time increment was determined by trial to be in the range of 3–6 μsec. Taking critical time increment as 3 μsec, for this particular case the solution reached steady state at the end of 3000 time steps.

A computer program was developed to plot the calculated results in graphical form [29]. The plotted transient data for the gas-phase temperature at axial position $z = 0.36$ (Fig. 7) indicate that a relatively cold gaseous oxygen supply from the

inlet actually blows out the flame which has been initially started. This fact is further demonstrated by the plotted transient data for the mass fraction of Al_2O_3 at the same axial position shown in Fig. 8.

C. *Second Set of Calculations—Flame Sustained*

It was pointed out by Kassoy and Williams [30] that the reaction orders for the fuel and oxidizer are not necessarily the same as the corresponding stoichiometric coefficients for a one-step overall reaction. It appears that the overall reaction orders should be determined either experimentally or through a detailed analysis of the actual reaction mechanism. Since both experimental data and reaction mechanism for the gas phase aluminum–oxygen reaction are not available at the present, arbitrary values were selected for the purpose of demonstrating that a flame could be sustained.

If the reaction, $2Al + O_2 \rightarrow 2AlO$, is assumed to be the rate-controlling step for the overall reaction of $2Al + 1.5O_2 \rightarrow Al_2O_3$, then, from the stoichiometric coefficients, 2.0 and 1.0 in place of 2.0 and 1.5 may be selected as the overall reaction orders, with respect to aluminum and oxygen. With these modified reaction orders, a second set of numerical calculations was performed which yielded the following results.

The transient gas-phase temperatures at axial position $z = 0.36$, are plotted in Fig. 9. At the start of the combustion process, the spontaneous chemical reaction increases the temperature of the initially ignited gas. As the relatively cold oxygen supply from the inlet reaches this axial position, the corresponding cooling effect is observed. Also, the position of the flame, as indicated by the peak of the temperature profile, is being pushed towards the fuel surface and is confined in a very narrow region within the turbulent boundary layer as the combustion continues.

The corresponding transient variation of the mass fraction of Al_2O_3 is plotted in Fig. 10. Initially no aluminum oxide was present. As combustion takes place, aluminum oxide is produced in the reaction zone as expected and increases with time.

The transient effect on the axial velocity profile due to mass addition and combustion is demonstrated in Fig. 11. Mass addition and combustion tend to decrease the magnitude of the axial velocity near the fuel surface.

The steady-state profiles of the axial and radial velocity components are plotted in Figs. 12 and 13, respectively. Since mass addition and combustion are more dominant in the downstreams, the magnitude of the axial velocity near the fuel surface decreases in the same direction. This phenomena is in qualitative agreement with the findings of Jones and Isaacson [17] in their experimental study of the reactive turbulent boundary layer.

Because the vaporization process alone contributes to the mass addition of fuel,

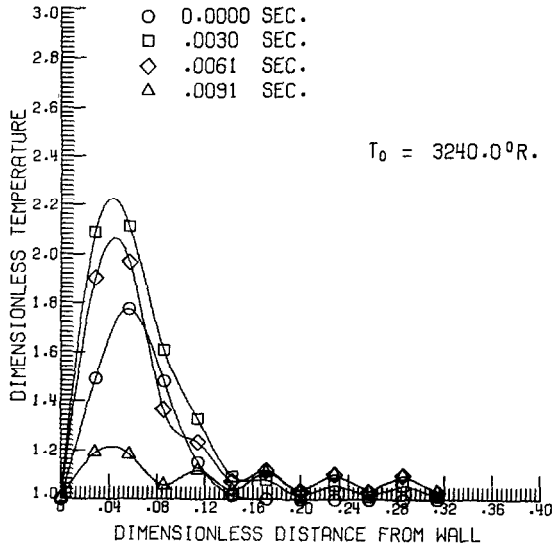

FIG. 7. Transient profiles of gas-phase temperature at axial position, $z = 0.36$—flame subsided.

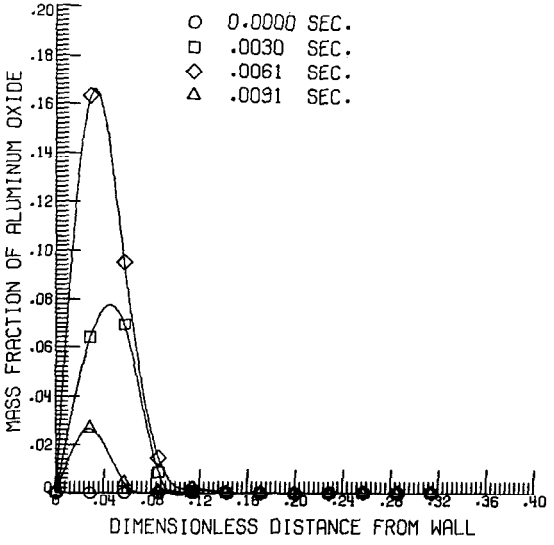

FIG. 8. Transient profiles of the mass fraction of Al_2O_3 at axial position, $z = 0.36$—flame subsided.

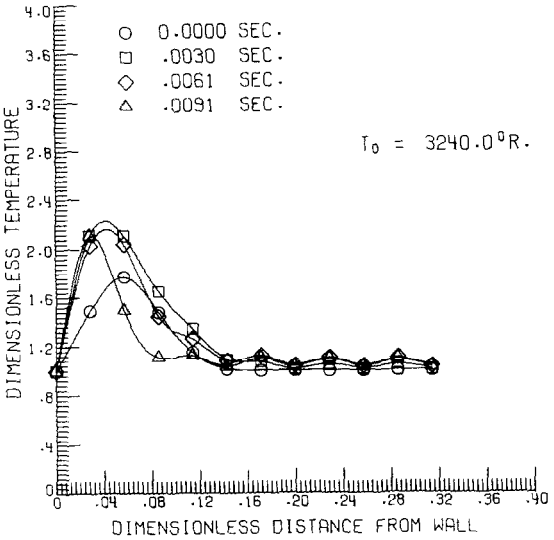

FIG. 9. Transient profiles of gas-phase temperature at axial position, $z = 0.36$—flame sustained.

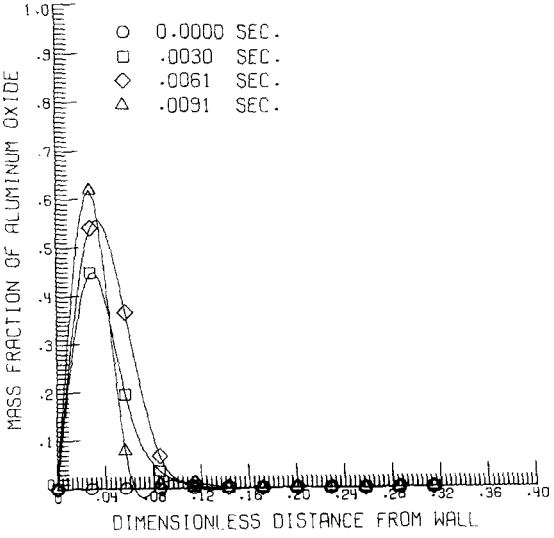

FIG. 10. Transient profiles of the mass fraction of Al_2O_3 at axial position, $z = 0.36$—flame sustained.

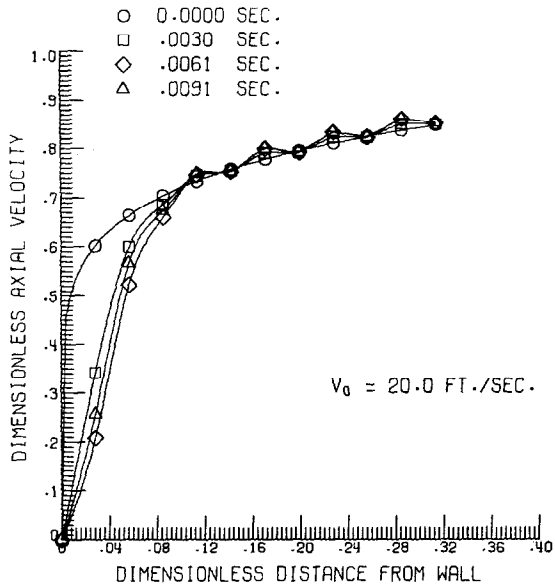

FIG. 11. Transient profiles of axial velocity component at axial position, $z = 0.36$—flame sustained.

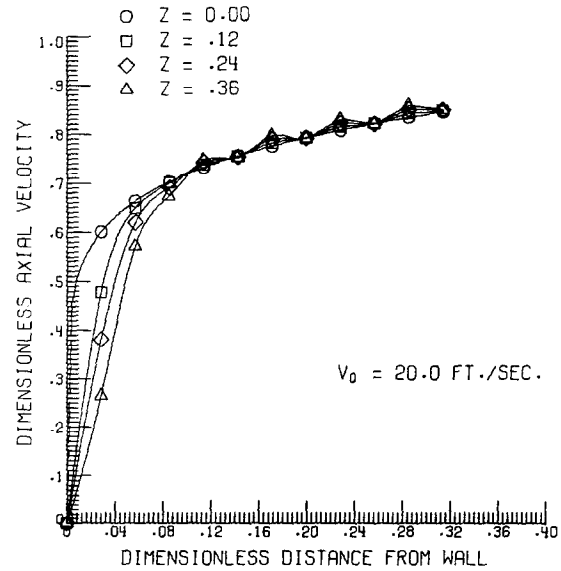

FIG. 12. Steady-state profiles of axial velocity component—flame sustained.

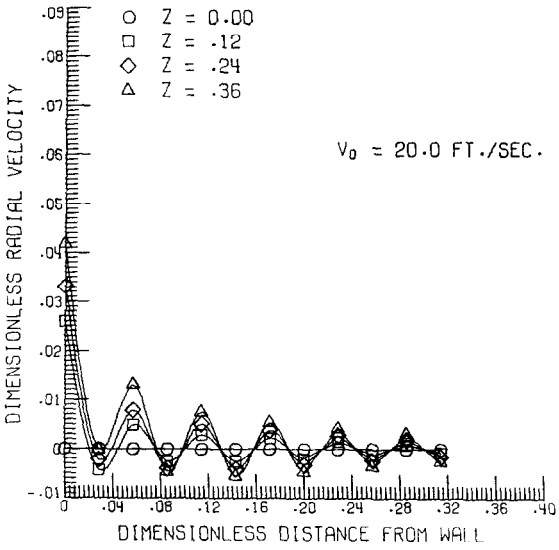

FIG. 13. Steady-state profiles of radial velocity component—flame sustained.

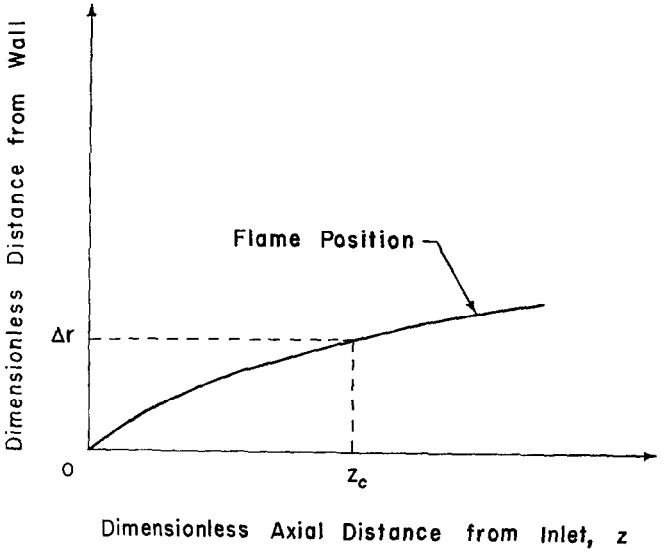

FIG. 14. Steady-state flame position in hybrid rocket combustion chamber.

the radial velocity component is expected to diminish to zero a short distance from the fuel surface. But due to the coarse grid spacings used, the finite difference method can only approximate the solution, with values fluctuating around zero. This fluctuation propagates downstream as observed in Fig. 13. These fluctuating values of radial velocity component in turn produce the ripples observed in some other plots indicating the strong coupling effect between these variables.

The Schlieren and shadowgraph studies by Muzzy [31] and a colored movie produced by ONERA [32] on experimental hybrid rocket systems demonstrated that the distance of the flame position from the fuel surface is zero at the inlet and increases in the downstream axial direction as shown in Fig. 14. If Δr is the dimensionless radial-grid spacing used in the finite-difference method, the flame position can be first detected a distance approximately equal to z_c downstream of the inlet.

The steady-state profiles of temperature in the gas phase are plotted in Fig. 15. The steady-state results indicate that the sustaining flame actually starts from a normalized distance, 0.32, which is 0.96 in. downstream of the inlet. From these steady-state profiles of temperature in the gas phase, the conductive heat flux to the solid wall as a function of the axial distance can be estimated, since the local burning rate of fuel is proportional to the conductive heat flux. The preliminary results shown in Fig. 15 indicate that the conductive heat flux to the solid wall appears to be constant between normalized axial distance, $z = 0.32$ and $z = 0.36$.

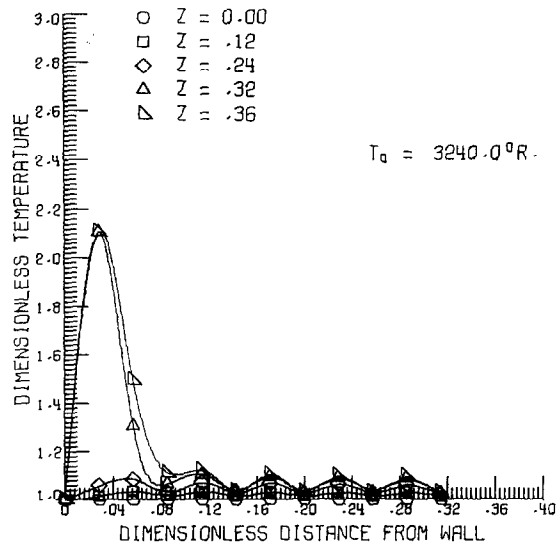

FIG. 15. Steady-state profiles of temperature in the gas phase.

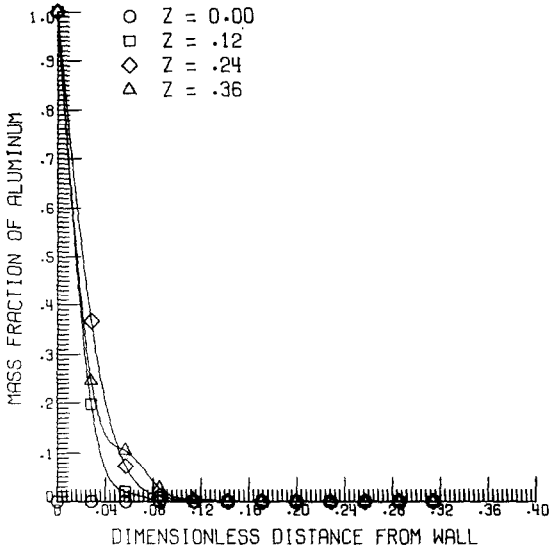

FIG. 16. Steady-state profiles of the mass fraction of aluminum.

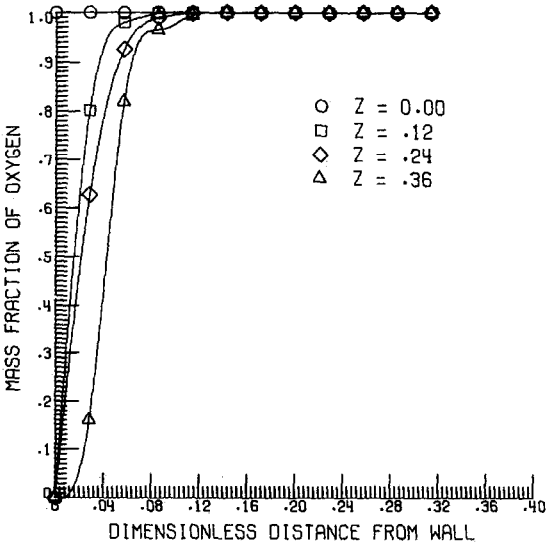

FIG. 17. Steady-state profiles of the mass fraction of oxygen.

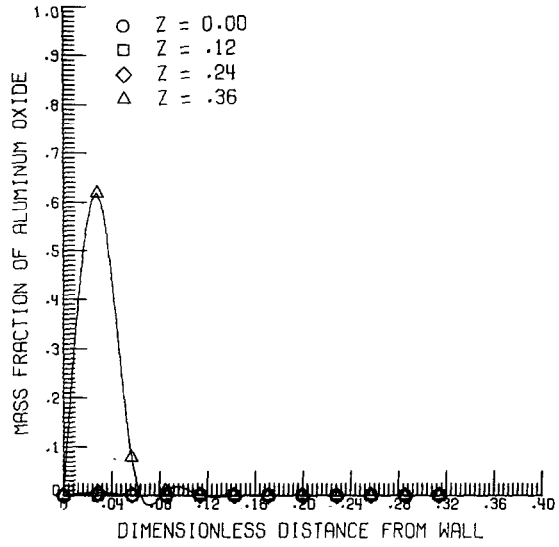

FIG. 18. Steady-state profiles of the mass fraction of aluminum oxide.

This is in agreement with the assumption of a constant burning rate. Hence, the constant burning rate assumption appears to be valid for solution over a short length of the combustion chamber. Since further development is planned in the future, the calculations have not been performed further downstream.

The steady-state profiles of the mass fractions of aluminum, oxygen, and aluminum oxide are plotted in Figs. 16–18, respectively. The sum of the mass fractions of aluminum, oxygen, and aluminum oxide at any grid point should add up to unity and this is remarkably obeyed within the convergence criteria used. As expected, pronounced production of Al_2O_3 with a corresponding depletion of aluminum and oxygen are observed in the sustaining flame zone.

Since the initial temperature profile in the solid phase was assumed to be that of a steady-state case at the start of the combustion process, the solution for the temperature in the solid phase is insignificant, and, therefore, not included.

CONCLUSIONS AND PLANS FOR FURTHER DEVELOPMENT

An overall approach has been followed to study the nonequilibrium aspects of reactive fluid flows in a hybrid rocket system through the use of numerical computation methods. The major contributions from the present study can be summarized as follows:

(a) A computational method has been developed which is capable of solving

the complete set of transient, two-dimensional, conservation equations for a reacting gas mixture with certain assumptions made.

(b) It has been further demonstrated that this system of equations is capable of handling the nonequilibrium aspects resulting from the turbulent flow of an oxidizer over solid fuel, with time-averaged turbulent property restriction.

(c) The transient solutions obtained indicate a smooth transition from initial to steady-state conditions, allowing a study of the transient phenomena in the hybrid rocket systems within a reasonable amount of computing time.

(d) The calculated results indicate that a flame is formed very close to the fuel surface, and, that there is a decrease in the magnitude of the axial velocity near the fuel surface.

(e) The calculated steady-state conditions indicate good qualitative agreement with available experimental data.

(f) As more sophisticated theoretical models are developed, it is expected that this computational method can be used to simulate experimental conditions more realistically.

Further computations are planned using this computer program [29] as a basic tool.

(a) A different fuel-oxidizer combination will be selected instead of aluminum–oxygen to establish the benchmark values for a new chemical combination.

(b) In order to give more physical meaning to the results, the mass addition from fuel surface will be modified to make it a function of the temperature at the fuel surface T_w,

$$\dot{r} = A \exp(-E_s/RT_w), \tag{33}$$

where A and E_s are empirical constants.

(c) It has been concluded that the radiative heat transfer from the hot combustion flame to the fuel surface should not be neglected when metallic fuel is used in a hybrid rocket system. Such effects can be accounted for by including an additional term in the energy balance equation.

(d) Since turbulent flow and extreme temperature gradient are characteristics of hybrid rocket systems, the assumption of constant properties is rather unrealistic. Hence, the effects of temperature and position dependence of variable fluid and transport properties will be investigated. Position dependence will be consistent with the definition of eddy viscosity in a developed pipe flow.

List of Symbols

C_p	Specific heat per unit mass of gas mixture at constant pressure
C_s	Specific heat per unit mass of solid fuel
D_a	Damkohler number, $r_0 W_0/\rho_0 v_0$
D_i	Binary diffusion coefficient of the ith chemical species into the rest
Ec	Eckert number, $v_0^2/C_{p0}T_0$
h	Enthalpy per unit mass of gas mixture
h_i^0	Heat of formation per unit mass of the ith chemical species
h_{Li}	Latent heat per unit mass of the ith chemical species due to phase change
P	Static pressure of gas mixture
Pr	Prandtl number, $C_{p0}\mu_0/\lambda_0$
r	Radial distance
$\dot{r}$	Regression rate of fuel surface
R_i	Gas constant of the ith chemical species
Re	Reynolds number, $r_0\rho_0 v_0/\mu_0$
Sc	Schmidt number, $\mu_0/\rho_0 D_0$
t	Time
T	Temperature of gas mixture
T_s	Temperature of solid fuel
v_r	Radial velocity component
v_z	Axial velocity component
W_i	Rate of production of the ith chemical species per unit volume
y_i	Mass fraction of the ith chemical species
z	Axial distance
α	Thermal diffusivity, $\lambda/\rho C_p$
λ	Thermal conductivity
μ	Viscosity of gas mixture
ρ	Density of gas mixture

Subscripts

i	The ith chemical species in the gas mixture
s	The corresponding value for solid fuel
w	The corresponding value at the gas-solid interface
o	The characteristic value

Acknowledgments

The authors are grateful to the financial support provided by NASA Grant No. NGR-47-005-085 which was monitored by Dr. A. R. Saunders of NASA, Langley Research Center.

Initial computation was carried out at the University of Virginia's Computer Science Center through a research grant. The major computation was performed through the generous computing time provided by the NASA Langley's CDC 6400/6600 computing facility.

REFERENCES

1. H. R. BARTEL AND W. D. RANNIE, "Solid Fuel Combustion as Applied to Ramjets," Progress Report 3-12, Jet Propulsion Laboratory, California Institute of Technology, Pasadena, CA, 1946.
2. S. S. PENNER, "Chemical Rocket Propulsion and Combustion Research," pp. 145–153, Gordon and Breach, New York, 1962.
3. S. FINEMAN, "Some Analytical Considerations of the Hybrid Rocket Combustion Problem." M. S. thesis, Princeton University, Princeton, NJ, 1962.
4. LEON, GREEN, JR., Introductory considerations on hybrid rocket combustion, *in* "Progress in Astronautics and Aeronautics: Heterogenous Combustion," Vol. 15, pp. 451–484, Academic Press, New York, 1964.
5. L. D. SMOOT AND C. F. PRICE, "Regression Rate Mechanism of Nonmetallized Hybrid Fuel Systems," AIAA preprint 65-56, *Amer. Inst. Aero. Astro.*, New York, Jan. 25, 1965.
6. A. MOUTET AND M. BARRERE, Contribution à l'Étude de la combustion dans les fusées a litergol ou hybrides, *in* "Advances in Aeronautical Sciences," pp. 465–495, Pergamon Press, New York, 1961.
7. G. A. MARXMAN AND M. GILBERT, Turbulent boundary layer combustion in the hybrid rocket, *in* "Ninth Symposium (International) on Combustion," pp. 371–384, Academic Press, New York 1963.
8. G. A. MARXMAN, C. E. WOOLDRIDGE, AND R. J. MUZZY, Fundamentals of hybrid boundary-layer combustion, *in* "Progress in Astronautics and Aeronautics: Heterogeneous Combustion," pp. 485–522, Academic Press, New York, 1964.
9. G. A. MARXMAN, Combustion in the turbulent boundary layer on a vaporizing surface, *in* "Tenth Symposium (International) on Combustion," pp. 1337–1362, The Combustion Institute, Pittsburgh, PA, 1965.
10. J. O. HIRSCHFELDER, C. F. CURTISS, AND R. B. BIRD, "Molecular Theory of Gases and Liquids," John Wiley and Sons, New York, 1954.
11. LESTER LEES, "Convective Heat Transfer with Mass Addition and Chemical Reactions," Third AGARD Combustion and Propulsion Panel Colloquium, Sicily, 1958.
12. P. M. CHUNG, Chemically reacting nonequilibrium boundary layers, *in* "Advances in Heat Transfer" (J. P. Hartnett and T. F. Irvine, Jr., Eds.), Vol. 2, Academic Press, New York, 1965.
13. R. B. BIRD, W. E. STEWART, AND E. N. LIGHTFOOT, "Transport Phenomena," John Wiley and Sons, New York, 1965.
14. D. U. VON ROSENBERG, "Methods for the Numerical Solution of Partial Differential Equations," American Elsevier, New York, 1969.
15. [illegible]
16. R. P. WILSON, JR., "Studies on Combustion of Aluminum Particles," Paper WSCI 69-5, Combustion Institute, Spring Meeting, China Lake, CA, 1969.
17. J. W. JONES AND L. K. ISAACSON, "A Turbulent Boundary Layer with Mass Addition, Combustion and Pressure Gradients," AFOSR Scientific Report AFOSR 70-1428TR, University of Utah, Salt Lake City, Utah 1970.
18. D. C. HODGMAN, R. C. WEAST AND S. M. SELBY (Eds.), "Handbook of Chemistry and Physics" (42nd ed.), The Chemical Rubber Publishing Co., Cleveland, OH, 1960.
19. K. R. VON HORN, (Ed.), "Aluminum," Vol. 1, p. 17, American Society for Metals, Metals Park, OH, 1967.
20. E. F. OBERT, "Concepts of Thermodynamics," p. 494, McGraw-Hill, New York, 1960.

21. A. V. GROSSE AND J. B. CONWAY, Combustion of Metals in Oxygen, *Ind. Eng. Chem.* **50** (1958), 667.
22. BERNARD CRAMPEL, "Chemistry of Propellant Constituents," ONERA-Note, Technique-113, Office National d'Études et de Recherches Aérospatiales, Paris, France, 1967.
23. R. R. ROTHFUS, D. H. ARCHER, AND K. G. SIKCHI, Distribution of Eddy Viscosity and Mixing Length in Smooth Tubes, *Amer. Inst. Chem. Eng. J.* **4** (1958), 27–32.
24. L. D. SMOOT AND D. F. PRICE, Regression Rates of Metalized Hybrid Fuel Systems, *A.I.A.A.J. Amer. Inst. Aero. Astro. J.* **4** (1966), 910–915.
25. C. E. WOOLDRIDGE AND R. J. MUZZY, "Internal Ballistic Considerations in Hybrid Rocket Design," AIAA 2nd Propulsion Specialists' Conference, Colorado Springs, CO, June, 1966.
26. C. E. BARNETT AND R. R. HIBBARD (Eds.), "Basic Considerations in the Combustion of Hydrocarbon Fuels with Air," N.A.C.A. Report 1300, Lewis Flight Propulsion Laboratory, Cleveland, OH, 1959.
27. H. BASSOW, "Construction and Use of Atomic and Molecular Models," Pergamon Press, New York, 1968.
28. J. O. HIRSCHFELDER, Semi-empirical calculations of activation energies, *J. Chem. Phys.* **9** (1941), 645–653.
29. W. S. Y. HUNG, "Theoretical Study of Reactive Fluid Flow in Heterogeneous Combustion Processes," Ph.D. dissertation, University of Virginia, Charlottesville, VA, 1971.
30. D. R. KASSOY AND F. A. WILLIAMS, Effects of chemical kinetics on near equilibrium combustion in nonpremixed systems, *Phys. Fluids* **2** (1968), 1344.
31. R. L. MUZZY, Schlieren and Shadowgraph Studies of Hybrid Boundary Layer Combustion, *Amer. Inst. Aero. Astro. J. A.I.A.A.J.* **1** (1963), 2159–2160.
32. "Combustion Visualization in Hybrid Rockets," Office National D'Études et de Recherches Aérospatiales, Paris, France, ONERA-Film-581, 1968.